Journal of Marine Research, 65, 589–605, 2007

Journal of
MARINE RESEARCH

Volume 65, Number 5

The ENSO signature in sea-surface temperature in the Gulf of California

by Hugo Herrera-Cervantes[1,2], Daniel B. Lluch-Cota[1], Salvador E. Lluch-Cota[1,3] and Guillermo Gutiérrez-de-Velasco S[2]

ABSTRACT

We analyzed 21 years of sea-surface temperature satellite images to explore the spatial signature of the El Niño-Southern Oscillation signal in the Gulf of California. We used empirical orthogonal function analysis to extract the principal mode of the nonseasonal sea-surface temperature variability and compared it to the spatial signature of the Southern Oscillation Index. The first mode accounted for 80% of nonseasonal variability and its amplitude time series was significantly correlated to the Southern Oscillation Index ($r = -0.58$, $P < 0.01$). The amplitude of this mode and its statistical relation to the El Niño is stronger during winter, which suggests that forcing of sea-surface temperature variability occurs through the disruption of the wind-driven upwelling corridor along the eastern coast due to El Niño-related atmospheric teleconnections. We also examined weekly time series of coastal sea-surface temperature coastal anomalies along the coast of North America, including the interior of the Gulf of California, during the strong 1997–98 El Niño. We found a poleward propagating signal that reached the mouth of the Gulf of California at the end of spring and continued its poleward propagation along the west coast of the peninsula slightly delayed; it also resulted in warming inside the Gulf of California. This observation may provide an explanation for the variable extension of the El Niño signature along the Pacific coast of North America.

1. Introduction

The Gulf of California (GC) is a subtropical, semi-closed sea with unrestricted communication with the Pacific Ocean. It is located between mainland Mexico and the

1. Centro de Investigaciones Biológicas del Noroeste (CIBNOR). P.O. Box 128, La Paz, Baja California Sur, México 23000.
2. Unidad La Paz, Centro de Investigación Científica y de Educación Superior de Ensenada, La Paz, Baja California Sur, México 23050.
3. Corresponding author. ***slluch@cibnor.mx***

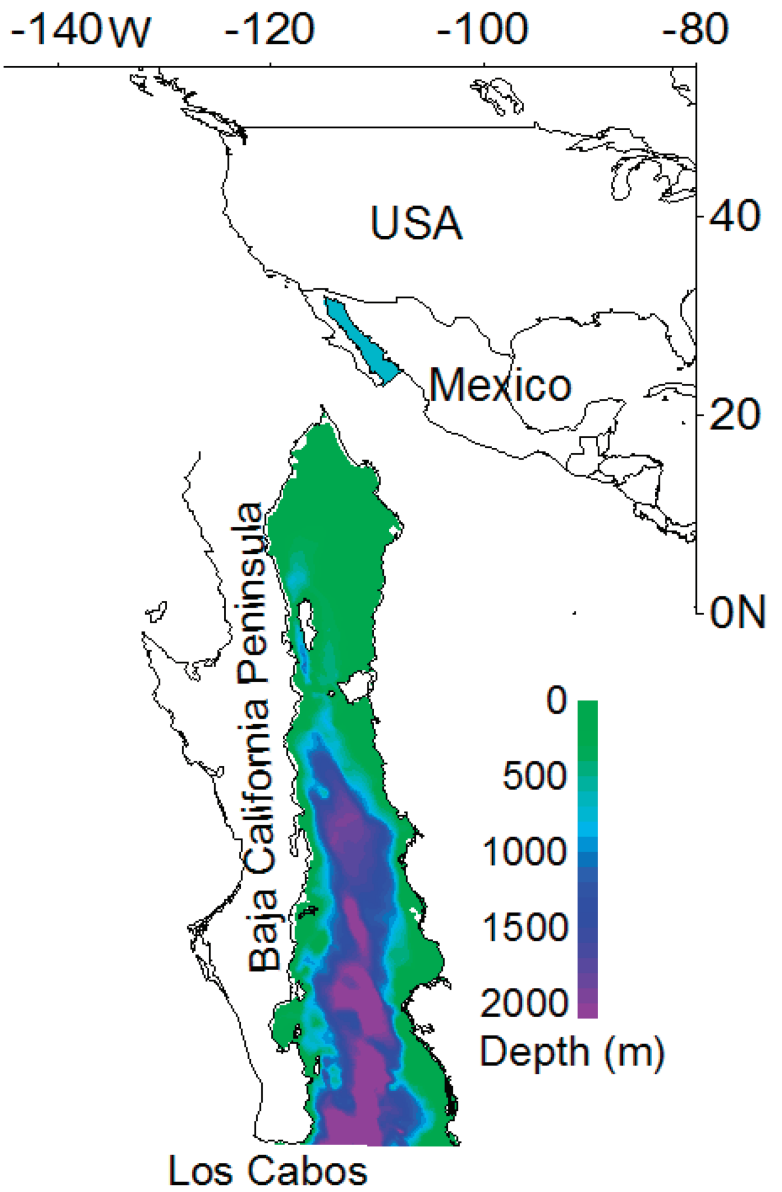

Figure 1. Location and bathymetry of the Gulf of California.

narrow Baja California peninsula (Fig. 1). Its climate results from remote and local heating and wind stress forcing that interact to produce a complex environment and a strong variability in its physical and biological processes (Baumgartner and Christensen, 1985; Ripa, 1997; Lluch-Cota *et al*., 2007)

Atmospheric circulation near the sea-surface level is largely monsoonal, with winds flowing from the northwest during winter and from the southeast during summer (Douglas *et al*., 1993). This pattern occurs because the mountain chains over both coasts cause wind to be funneled along the Gulf's longitudinal axis (Parés-Sierra *et al.*, 2003). The GC is divided in two by the Midriff Islands: a shallow northern area that is mostly controlled by local climate and tidal dynamics and a deep southern portion mostly influenced by the Pacific Ocean (Marinone, 1988). High biological productivity results from enrichment processes due to tidal mixing and wind-driven coastal upwelling along the eastern coast during winter (Lluch-Cota, 2000).

Interannual variability in physical and biological processes is also present in the GC (Lluch-Cota *et al*., 2007). Several studies of the basin-wide distribution of physical variables have shown warm temperatures, high sea levels, and low salinity during El Niño episodes (Robles and Marinone, 1987; Marinone, 1988; Lavín *et al*., 2003). However, the effects of El Niño on primary and secondary producers is less clear; some authors reported reductions in phytoplankton (Thunell, 1998; Santamaría-del-Angel and Alvarez-Borrego, 1994; Kahru *et al.*, 2004), whereas others report no significant changes in phytoplankton or zooplankton populations (Valdez-Holguín, 1986; Alvarez-Borrego and Lara-Lara, 1991) or zooplankton (Jiménez-Pérez and Lara-Lara, 1988; Lavaniegos-Espejo and Lara-Lara, 1990).

Two physical mechanisms are thought to contribute the most to the link between the GC and ENSO (Strub and James, 2002): (1) increased poleward (or decreased equatorward) winds caused by changes in the midlatitude atmospheric circulation related to ENSO through atmospheric dynamics (Emery and Hamilton, 1985; Latif and Barnett, 1994) and (2) poleward advection along the ocean-continent boundary, which form a wave guide for various modes of coastal trapped waves (Parés-Sierra and O'Brien, 1989; Subbotina *et al.*, 2001). Regarding the potential propagation of coastal waves along the coast of North America, Bakun (1996) noted that waves would have to somehow bypass the interruption in the coastal wave guide caused by the entrance to the GC or travel into and around one or more of the interior topographic basins and then re-emerge at the tip of the Baja California peninsula to continue poleward.

Lluch-Cota *et al.* (2001, 2003) and Strub and James (2002) analyzed records of sea-surface temperature (SST), sea-surface height (SSH), and geostrophic transport in connection with the propagation of ENSO signals along the coast of North America. They noted that changes along the coast are caused both by propagation of signals from the south (stronger between the equator and the entrance to the Gulf of California) and by local and basin-scale winds (stronger between the Pacific Northwest and the Alaska Peninsula). However, the spatial resolution of the data prevented them from including variability inside the GC in their analyses.

Several authors have analyzed GC variability from satellite-derived SST data with high spatial resolution but relatively short temporal coverage. For example, Soto-Mardones *et al.* (1999) and Lavín *et al*. (2003) examined the seasonal and interannual SST variability

for different periods (1984–1995 and 1984–2000, respectively). They found that changes related to both cold and warm ENSO episodes were evident in the central region south of the Midriff Islands but not in the northern GC. Lavín *et al*. (2003) also compared a spatially averaged anomaly series of the GC to the Southern Oscillation Index (SOI) and found a significant relationship during the strongest ENSO events.

In this work, we extend the analysis of Lavín *et al.* (2003) using a longer satellite-derived SST dataset. First, we use empirical orthogonal function (EOF) analysis to extract the principal mode of the nonseasonal SST variability (EOF_1) and compare the time series to the SOI. Then we compared the spatial pattern of this main mode to that of ENSO using linear regression analysis (LRA). Finally, we examine weekly time series of coastal SST anomalies, including the inside of the GC to investigate its effects on the propagation of the ENSO signal during the strong 1997–1998 El Niño.

2. Data and methods

The main data used in this analysis are monthly composites of SST satellite images from January 1984 to December 2004. The area of interest is the Gulf of California and the Pacific coast of North America between 10N to 40N (see Fig. 1).

For the period 1984–2000 we used the data set compiled by Lavín *et al*. (2003) from data provided by the Physical Oceanography Distributed Active Archive Center (PO.DAAC, webpage http:// podaac.jpl.nasa.gov). To update this dataset we used 225 daily images obtained from afternoon passes of the NOAA-12 and NOAA-16 satellites over the area of interest between January 2001 and December 2004. These images were provided by the CICESE-BCS Satellite Oceanography Station (http://www.cicese.mx/lapaz/catalogo2). Only cloud-free images were selected using the criteria provided by Paden *et al*. (1991). After masking land and clouds and rotating the images, 18 x 18 km pixel arrays were averaged to produce monthly SST composites with the same spatial resolution used by Lavín *et al*. (2003).

This process resulted in a matrix of SST(x,t) values, where x stands for the pixels within each image and t stands for each month between January 1984 and December 2004. To remove the seasonal signal, we fitted the monthly time series of each pixel to the periodic function as follows:

$$\mathbf{S}(t) = A_0 + A_1\cos(w_1 t - \varphi_1), \tag{1}$$

where A_0 is the annual mean; A_1, w_1, and φ_1 are the amplitude, frequency, and phase of the annual signal. Next, we obtained a matrix of temperature anomalies (i.e., nonseasonal variability) as:

$$\mathbf{TA}(x, t) = \mathbf{SST}(x, t) - \mathbf{S}(x, t). \tag{2}$$

This matrix was transformed into one of normalized anomalies **NA**(x,t) by dividing the **TA**(t) series of each pixel by its standard deviation, (i.e., series were re-scaled to make

them comparable). We analyzed the resulting **NA**(x,t) matrix using EOF analysis to identify the main modes of SST nonseasonal variability. To investigate the potential connections of this variability to ENSO, we applied the EOF analysis to the complete data set and also to two subsets, one of winter values (December to January) and the other of summer anomalies (June to August). For a comprehensive description of EOF analysis, see Peixoto and Oort (1992) and Wilks (1995).

The spatial signature of the ENSO in the GC was revealed using LRA. We computed the simple linear regression between each **NA**(t) series and the SOI. We applied this procedure to the two subsets. SOI series was obtained from the Climate Prediction Center of the National Center of Environmental Prediction at the National Oceanic and Atmospheric Administration (CPC-NCEP-NOAA) website (http://www.cpc.ncep.noaa.gov). In the SOI series, warm El Niño (cold La Niña) episodes corresponded to negative (positive) SOI values; thus, we normalized and reversed the sign of the SOI values prior to the LRA to make a direct comparison with local temperature changes. For comparison, we used the "Tropical Pacific Cold and Warm Episodes by Season" list compiled by the CPC-NCEP (available at http://www.cpc.ncep.noaa.gov/ products/analysis_monitoring/ensostuff/ ensoyears.shtml), to identify ENSO episodes during the analyzed period.

Finally, we examined SST time-series data since January to December of 1997 within 50 km of the coast of North America (10N to 40N) including the east and west coasts of the GC. For this analysis, we used SST weekly 18 x 18 km pixel arrays composites filtering out the seasonal cycle subtracting the SST weekly climatology provided by the NOAA/NASA AVHRR Oceans Pathfinder sea-surface temperature data (PO.DAAC, webpage http:// podaac.jpl.nasa.gov). After computing weekly anomalies, we normalized the series in the same way that the monthly composites to build time plots of SST anomalies along the coast (Hovmöller diagrams).

3. Results

Figure 2 shows a surface plot (time-averaged **SST**$(x,\tilde{t})$ values) and a time plot (space-averaged **SST** $(x,\tilde{t})$) of the satellite-derived SST observations in the GC. As would be expected, SST followed a latitudinal gradient that is particularly evident at the southern deep basin. Relatively cool conditions exist around the Midriff Islands and in the shallow northern area due to strong tidal mixing. This produces a persistent pool of cold water in the Midriff Island region spreading through advection and horizontal mixing and resulting in a general cooling of the northern gulf that creates large temperature gradients (Paden *et al*., 1991). SST time variability was dominated by a strong seasonal cycle, although large interannual changes were still evident during ENSO events (Fig. 2; lower).

Figure 3 shows the eigenvalues of the first five EOFs from the **NA**(x,t) matrix (i.e., after removing the seasonal signal). SST interannual variability in the GC clearly conformed to a single dominant mode. EOF_1 accounted for 80% of the variance, and no other mode could be resolved because sampling errors were large enough to prevent neighboring eigenvalues from being statistically different (North *et al*., 1982).

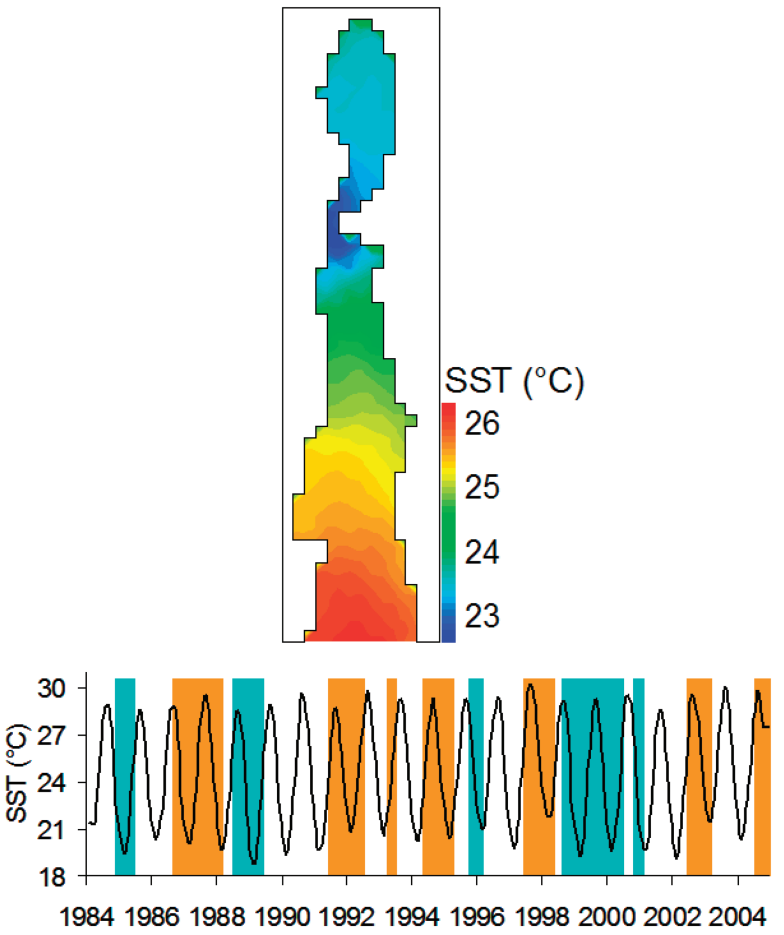

Figure 2. Surface plot (time averaged) and monthly time series (spatially averaged) of the satellite-derived SST observations. Shaded areas indicate El Niño (red) and La Niña (blue) episodes as reported by the Climate Prediction Center of the National Center of Environmental Prediction at the National Oceanic and Atmospheric Administration (CPC-NCEP-NOAA).

Figure 4 shows the spatial pattern of this single dominant mode as surface plot of the EOF_1 loadings (upper panel) and the amplitude time series (time plot of the EOF_1 scores; lower panel). Over time, the SST interannual variability in the GC was forced by ENSO-related events (e.g., the signals of the 1988–89 La Niña, 1991–1992 and 1997–98 El Niño). This variability was not spatially homogeneous but tended to be high along the east coast and south of the Midriff Islands as compared to the coast of the peninsula and the northern area. The figure also shows the time series of the (negative) SOI index and its spatial signature as the surface plot of the *R* values obtained from the linear regression of each **NA**(*t*) series to the –**SOI**(*t*) (Fig. 4; lower). Although the *R* values indicate a weak

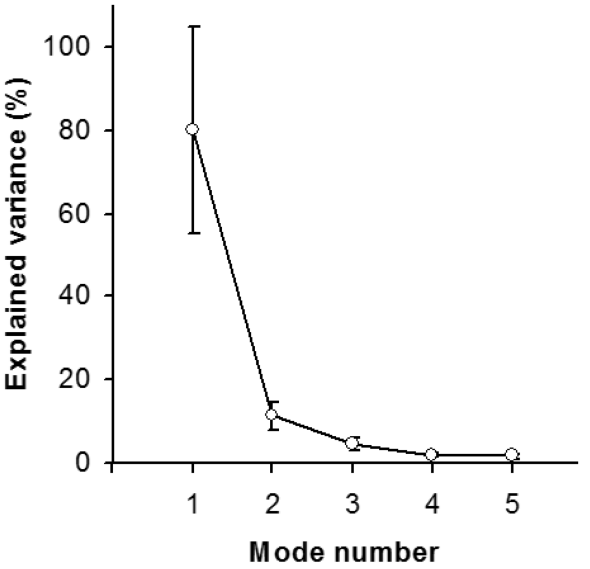

Figure 3. Graph of the first five Empirical Orthogonal Functions (modes) indicating percent of explained variance and standard deviation error bars (sampling error).

statistical relationship between the –**SOI**(t) and the individual **NA**(t) series ($R = 0.28$ to 0.38), their spatial patterns were close to that of the EOF_1. In agreement, the EOF_1 series and the –**SOI**(t) showed similar trends and were well correlated ($r = 0.58$, $P < 0.01$).

Figure 5 shows the spatial patterns of the EOF_1 for the subset corresponding to winter and summer anomalies. Winter EOF_1 accounted for 90% of the winter variance and showed a spatial signature close to those shown in Figure 4, with high values along the east coast and south of the Midriff Islands. The R values obtained from the linear regression of the individual **NA**(t) winter series to the –**SOI**(t) were significant ($R = 0.40$ to 0.57). For summer EOF_1 accounted for 77% of the variance (a percentage smaller than that for winter) and showed a different spatial pattern, with high values that appear to have stalled around the Midriff Islands and in some areas near the mouth of the GC. In this case, the R values obtained from linear regression indicated a weaker statistical relationship of the individual **NA**(t) summer series to the –**SOI**(t) ($R = 0.04$ to 0.45).

Figure 6 shows the time evolution of El Niño-1997 along the equator (2N) using the TAO/TRITON array data from January to December, 1997. Left panel represents SST anomalies and right panel heat content anomalies. Moored data show an anomalous early warm event, identified from early 1997 (March) and intensified from mid-1997 (June) through the end of the year and culminating in a mature phase with maximum SST anomalies around November-December 1997. Time-longitude contours of these variables showed that warm signal propagated eastward across the basin at Kelvin wave-like speeds reported by Chelton *et al*. (1998).

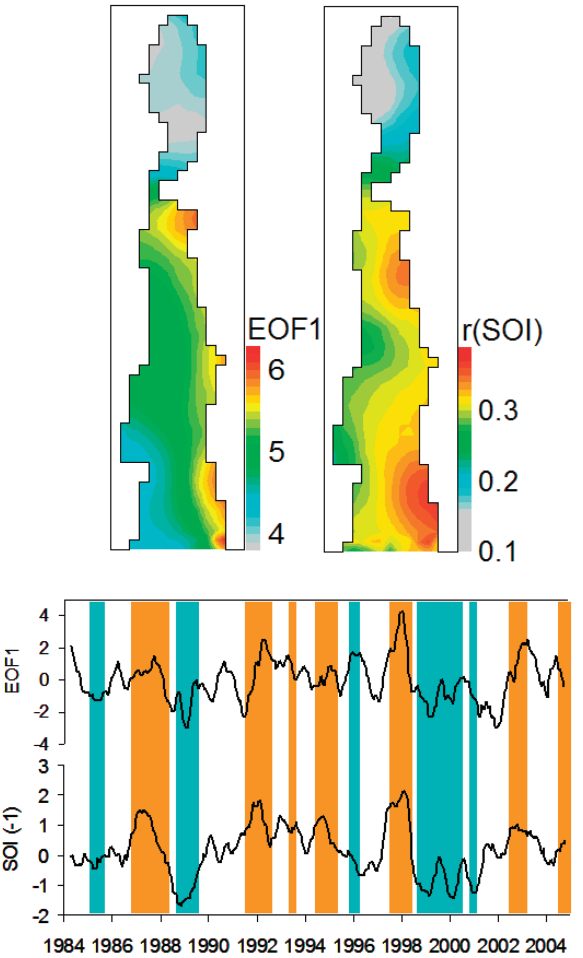

Figure 4. Surface plots of the EOF_1 of SST anomalies and the correlation coefficients from the linear regression between the SST anomalies and the sign-reversed SOI as the independent variable. Time-series data indicate the temporal evolution of the EOF_1 and the sign-reversed SOI, both smoothed by a five-term running mean. Shaded areas indicate El Niño (red) and La Niña (blue) episodes as reported by the Climate Prediction Center of the National Center of Environmental Prediction at the National Oceanic and Atmospheric Administration (CPC-NCEP-NOAA).

Figure 7 shows three Hovmöller diagrams of weekly averaged coastal SST anomalies from January to December 1997. Upper panel covers the coast from 10N to 40N but does not includes the GC. Although large portions of this diagram are affected by missing data due to cloudiness, a poleward propagation of warming anomalies from February (near 10N) to November (35N) is clearly evident. It should be noted that the signal reached the mouth of the GC at the end of spring (dashed line about 23N) and continued its poleward

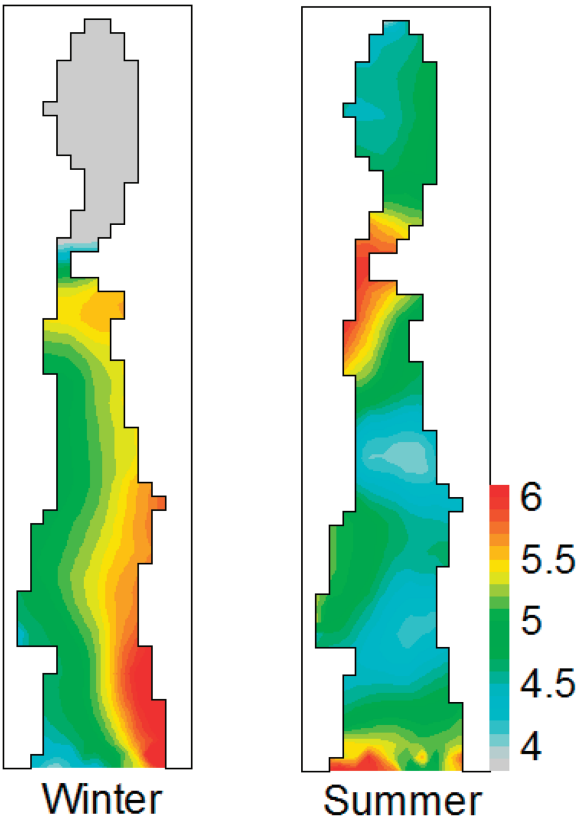

Figure 5. Spatial patterns of the EOF_1 of SST anomalies for (a) winter (December, January, and February) and (b) summer (June, July, and August).

propagation along the west coast of the peninsula, seemingly bypassing the mouth without any significant delay.

Middle panel shows the temporal evolution of the SST anomalies along the entire coastline inside the GC, from the mainland coast at the mouth (at the bottom of the graph) to the southern tip of the peninsula (at the top, the black line at the middle corresponds to the northernmost portion of the coast). Slope in the contours suggests that warming propagation in the Gulf took approximately 3 weeks (May–June) along both coasts of the Gulf (~3200 km). Using these scaling arguments the theoretical phase speed of this warm signal is ~150 km day^{-1}, resulting in warm anomalies that stalled south of the Midriff Islands (i.e., about the middle portion of each coast) and at the mouth of the GC, in a pattern that is similar to that found for the summer EOF_1 (Fig. 5).

Finally, the lower panel shows the coastal propagation of the warm signal both outside and inside the GC, created by combining the two previously described panels. This figure

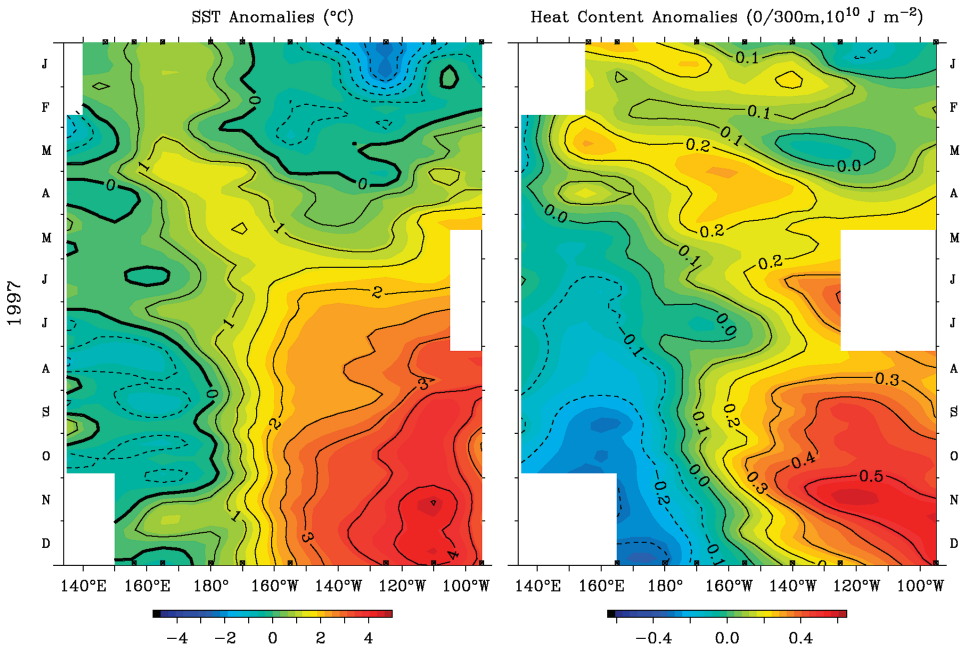

Figure 6. Time-longitude sections of weekly SST anomaly, and head content anomalies along 2°N from January to December 1997. The data are provided by TAO/TRITON project office/PMEL/ NOAA. Dotted contours indicate negative values.

shows that the warming anomalies appeared first at the south, and then propagated poleward along the coast, reaching the mouth of the GC at the end of spring, somehow bypassing the Midriff Islands and then reaching the tip of the peninsula, and continued along the west coast of the peninsula. Warming anomalies presented a slight attenuation poleward, north of 25N, and finally reinforced by strong anomalies, reported since October and November along the coast of California (Dever and Winant, 2002; Ryan and Noble, 2002).

4. Discussion

In this study, we analyzed satellite-derived SST data for the GC, which allowed us to examine SST interannual variability with a spatial resolution of 18 x 18 km for a relatively long period of time that includes several ENSO events. In addition, we followed the coastal propagation of the warming anomalies related to the very strong 1997 El Niño with a temporal resolution of one week and the same spatial resolution in monthly composites (18 km). To our knowledge, this is the first time that the possible effects of ENSO on SST inside the GC have been examined at this level of detail.

EOF analysis of the entire dataset (i.e., of the total variance) yielded a single dominant mode for the analyzed period (Fig. 3). The evidence linking this mode to ENSO variability

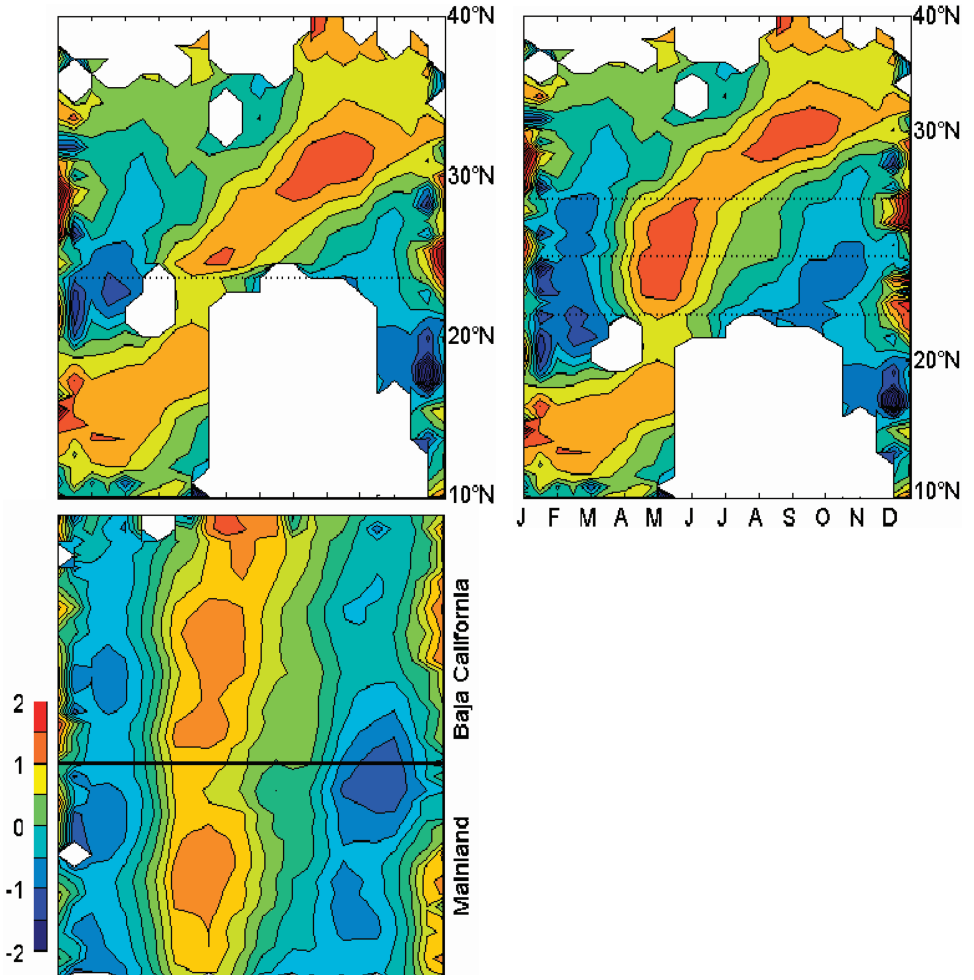

Figure 7. Hovmöller diagrams of weekly averaged coastal SST anomalies (values within 50 km of the coast) from January to December 1997 covering (a) the coast from 10N to 40N (white areas indicate missing data due to clouds and dotted line ~24N), (b) both coasts of the Gulf of California (the black lines indicate the northernmost portion of the Gulf coast), and (c) the two combined showing the coastal propagation of the signal both outside and inside the Gulf of California (dotted lines) and along the coast from 10N to 40N. Units of the color bar are in °C.

may seem contradictory. On one hand, we found a strong similarity between this mode and the spatial signature of ENSO as revealed by the linear regression of the SOI (Fig. 4). On the other, the statistical relationship between the SOI and the SST anomalies, accounted ~33% of the variance of the EOF_1 amplitude series. Beyond the obvious consideration that the SOI refers to a tropical atmospheric phenomenon only indirectly related to extra-tropical variability, the GC exhibits complex dynamics resulting not only from oceanic and

atmospheric forcing but also from dissipative phenomena related to winds stress, local topography, bottom friction, and tidal forcing (Ripa and Marinone, 1989). Any signal of the ENSO on SST would be masked by these local processes, thus obscuring their statistical relationships. Therefore, we believe that the similarity of the spatial patterns and the parallel trends between the series shown in Figure 4 indicate an important role of ENSO in forcing interannual variations in the GC.

Both spatial patterns, the EOF_1 and the linear regression of the SOI, show that variability is higher south of Midriff Islands and along the eastern coast where the continental shelf is wider (see Fig. 1), and wind-driven upwelling occurs during winter. Our interpretation of these patterns is that this similarity is indicative of the disruption of the wind-driven upwelling process during El Niño events, which may result from a weakening of the winds (i.e., from atmospheric teleconnections), from deepening of the thermocline due to coastal waves (an oceanic connection), or from both mechanisms. The fact that this spatial structure (EOF_1) and its statistical relation to the ENSO index is more evident when only the winter anomalies are considered (Fig. 5) suggesting that atmospheric teleconnections, mostly restricted to the winter (Tribbia, 1991), are major phenomena behind ENSO forcing of SST interannual variability in the GC.

Nevertheless, EOF analysis of the summer data subset revealed a spatial structure of high SST variability around of the Midriff Islands and near the mouth of the GC (Fig. 5). Although the physical processes that cause this pattern are not clear, the fact that a similar pattern emerged from the analysis of the coastal propagation of the 1997 El Niño warming inside the GC (Fig. 7, panel b) strongly suggests that this pattern may occur after the propagation of ENSO-related coastal waves into the GC. While the poleward propagation of coastal waves must occur along the east coast of the GC, the signal may be transmitted across the GC to its west coast over a period of three weeks (Beier, 1997) by propagation of coastal waves smoothed by bottom friction and masked by local dynamic.

Figure 7 clearly shows that the strong 1997 El Niño, the signal of coastal waves continued its poleward propagation along the west coast of the peninsula. Although ENSO effects in the northeast Pacific are most often related to basin-scale atmospheric teleconnections (Emery and Hamilton, 1985; Hollowed and Wooster, 1992; Wooster and Hollowed, 1995), some modeling studies have suggested that coastal waves generated during El Niño events can propagate poleward along California (Parés-Sierra and O'Brien, 1989) and reach latitudes as high as the Gulf of Alaska (Jacobs *et al*., 1994).

To understand the evolution of the warming signals associated with El Niño 1997, as shown in Figure 7, we computed the phase speed of internal Kelvin waves and internal Rossby radius of deformation, using expressions proposed by Gill (1982, p.122, 249) and hydrographic data monitored during 1997 in different points of continental shelf between 10N and 40N, including the GC (Filonov and Tereschenko, 2000; Amador-Buenrostro, *et al*.,2003; Durazo and Baumgartner, 2002; Dever and Winant, 2002; Ryan and Noble, 2002). The expression used for phase speed is $c_1 = (g' \cdot H_1 \cdot H_2/H_T)^{1/2}$, where g' is the reduced gravity calculated with typical density values in upper and lower layer, H_1 the

maximum thickness of upper layer, H_2 the thickness of lower layer and $H_T = H_1 + H_2$, mean depth of the continental shelf.

For the coastal region between 10N and 21N, where the continental shelf is narrow, phase speed was estimated at ~100 km day^{-1}, and internal Rossby deformation radius between 30 and 35 km (Filonov and Tereschenko, 2000). Time for a coastal wave traveling some 7600 km of coastline, from the equator to the mouth of the Gulf of California should be ~76 days. For inside the Gulf of California, we used $H_1 = 80$ m and $H_T = 730$ m, the mean depth of the Gulf (Beier, 1997). Typical values of phase speed for a coastal wave propagating to the interior the Gulf are ~140 km day^{-1}. Internal Rossby deformation radius corresponding to this phase speed is between 30 -21 km, smaller than the average width of the Gulf (~150 km). Signals associated with coastal waves travel around the Gulf (some 3200 km of coastline) in ~23 days and could be affected by friction, thus some dampening would be expected. For the northern coastline between 21N and 40N (~5,050 km), mean phase speeds were ~75 km day^{-1} and the internal Rossby deformation radius approximately 10 km. According to these computations, coastal wave take ~67 days to arrive at 40N.

Phase speed calculations as explained above suggest that a coastal signal generated near the equator and propagated poleward arrives at 40N in approximately 5 months. Figure 6 showed that the El Niño signal associated with an equatorial Kelvin wave arrived to the east boundary in March, generating a poleward propagation coastal wave. This signal arrived at the mouth of the Gulf in May, continuing its propagation along both coasts of the Gulf reaching the tip of the peninsula in the middle of June and continued poleward propagation along the west coast of the peninsula (north of 25N), reaching ~35N by July-August. A second episode of strong anomalies was observed at the end of 1997 (October- December) in the California coast.

Filonov and Tereschenko (2000) observed an El Niño signal in temperature profiles measured over the continental shelf at 19N in May and June. Dever and Winant (2002) showed that an El Niño initial signal arrived at Point Conception (34N), concentrated in the upper 25 m, by early-July. Ryan and Noble (2002), using time-series of daily SST anomalies near to 37N, observed the same evolution of the event and a reinforcement starting in November with no direct correlation to local winds. Dever and Winant (2002) and Strub and James (2002) suggest that this initial anomaly observed clearly in the Gulf was the northern tail of a coastally trapped Kelvin wave propagating poleward from Baja California (24N) and farther north during a transient event.

Outside the upwelling period during summer-fall, atmospheric effects may not result in large SST changes in the GC. First, atmospheric teleconnections are unlikely to occur in summer (Tribbia, 1991), and also surface winds in the GC reach their seasonal minima during this period (Parés-Sierra *et al.*, 2003), thus no major interannual warming would be expected from atmospheric effects. Multivariate ENSO Index shows that El Niño 1997 had a decline in the temperatures anomalies during August-October and intensified again from

mid-November through the end of the year (http://www.cdc.noaa.gov/people/klaus.wolter/MEI/).

The GC has the higher phase speed for a coastal trapped wave. This could explain the fact that the signal detected in May at the mouth of the Gulf (Fig. 7, central panel) takes about one month to travel around the Gulf. The contour slope in this panel suggests that the signal takes ~21 days (~150 km day^{-1}) very close to phase speed calculated above. Beier (1997), based on numerical experiments, concluded that the Pacific Ocean forces through incoming baroclinic waves in the mouth of the Gulf in phase with the wind stress; moreover, total circulation can be explained by means of an internal wave trapped against the wall that propagates around the coast of the Gulf. Strub and James (2002) proposed that high SSH during El Niño 1997 initially filled the lower Gulf and created a SSH gradients at the mouth of the Gulf that allowed geostrophic flows past the mouth and northward along Baja California.

Lluch-Cota *et al*. (2001) analyzed the variability of coastal SST along the Pacific coast of North America from 1950 to 1999, as revealed by the multiple linear regression of monthly SST anomalies to the Multivariate ENSO Index (MEI; Wolter and Timlin, 1993) and the Pacific Decadal Oscillation Index (Mantua, 2001). Lluch-Cota *et al*. (2001) illustrated that the highest latitude at which the partial regression of the MEI still explains a large fraction of the SST variability is not the same for every ENSO event. For most events, this latitude corresponded to the west coast of the Baja California peninsula, but for some others the signal reached the Gulf of Alaska. Strub and James (2002) demonstrated ENSO signal asymmetry is related to the influence of topographic features, local winds and local currents.

Our results clearly show that the GC plays a significant role in the poleward propagation of ENSO-related coastal waves. Internal Rossby deformation radius corresponding to phase speed values computed for the GC are narrower than the separation between the mainland coast and the southern tip of the Baja California peninsula. Coastal waves related to El Niño events would enter the GC along its eastern coast and would probably undergo a significant weakening through friction and dispersion as they travel into and around one or more of the interior topographic basins. On the other hand, if the amplitude and duration of strong El Niño events (as 1997-1998) result in more than one peak of persistent warm SST and thermocline depth anomalies, coastal trapped wave modes could generate more intense poleward advection. The first episode could enter the GC along both coasts and weaken due to friction and dispersion, leaving the Gulf at the southern tip of the peninsula some 3-4 weeks later, and continue its poleward propagation along the west coast. A second episode (2-3 months later) would be more consistent north of 24N and probably reach high latitudes.

This hypothesis is consistent with the observation that the poleward propagation of coastal SST anomalies during the 1997 El Niño seemingly bypassed the GC without any noticeable delay (Fig. 7) and may provide an explanation for the results of Lluch-Cota *et al*.

(2001) and Strub and James (2002) regarding the variable extension of the ENSO signature along the Pacific coast of North America.

5. Conclusions

ENSO is a major source of SST interannual variability in the GC. The spatial signature of ENSO suggests that its most significant effect is the disruption of the wind-driven upwelling corridor along the eastern coast of the GC. This signal is more evident during winter, which suggests that ENSO forcing of SST variability occurs through atmospheric teleconnections. Nevertheless, evidence on the propagation of SST coastal anomalies also suggests that ENSO-related coastal waves enter the GC; thus, the GC could play an important role in their poleward propagation along the longer and convoluted Pacific coast of North America.

Acknowledgments. This research was supported by PROJECT SEMARNAT-2002-C01-0278 and CIBNOR EP-3 grants. We thank M. Lavín (CICESE) for the SST monthly data and A. Parés-Sierra (CICESE) and E. Beier (CICESE-BCS) for their comments. E. González (CICESE-BCS) provided daily AVHRR-images. HHC is doctoral student at CIBNOR and holds a CONACYT scholarship (94964).

REFERENCES

Alvarez-Borrego, S. and J. R. Lara-Lara. 1991. The physical environment and primary productivity of the Gulf of California, *in* The Gulf and Peninsular Province of the Californias. B.R.T. Simoneit and J. P. Drophin, eds., American Association of Petroleum Geologists Memoir*, 47,* 555–567.

Amador-Buenrostro, A., A. Trasviña-Castro, A. Muhlia-Melo and M. A. Argote-Espinoza. 2003. Influence of EBES seamount and Farallón Basin on coastal circulation in the Gulf of California, México. Geofísica. Internacional, *42*, 407–418.

Bakun, A. 1996. Patterns in the ocean, *in* Ocean Processes and Marine Population Dynamics. California Sea Grant / Centro de Investigaciones Biológicas del Noroeste, La Paz, B.C.S., Mexico. 323 pp.

Baumgartner, T. R. and N. Christensen. 1985. Coupling of the Gulf of California to large-scale interannual climatic variability. J. Mar Res., *43*, 825–848.

Beier, E. 1997. A numerical investigation of the annual variability in the Gulf of California. J. Phys. Oceanogr., *27*, 615–632.

Chelton, D. B., R. A. de Szoeke, M. G. Schlax, K. El Naggar and N. Siwertz. 1998. Geographical variability of the first-baroclinic Rossby radius of deformation. J. Phys. Oceanogr., *28*, 433–460.

Dever, E. P. and C. D. Winant. 2002. The evolution and depth structure of shelf and slope temperatures and velocities during the 1997–1998 El Niño near Point Conception, California. Prog. Oceanogr. *54*, 77–103.

Douglas M. W., R. A. Maddox, K. Howard and S. Reyes. 1993. The Mexican monsoon. J. Climate*, 6,* 1665–1677.

Durazo R. and T. R. Baumgartner, 2002. Evolution of oceanographic condition off Baja California: 1997–1998. Prog. Oceanogr., *54*, 7–31.

Emery, W. and K. Hamilton. 1985. Atmospheric forcing of interannual variability in the northeast Pacific Ocean: Connections with El Niño. J. Geophys. Res., *90*, 857–868.

Filonov, A. and I. Tereshchenko. 2000. El Niño 1997–1998 monitoring in mixed layer at the Pacific Ocean near Mexico's west coast. Geophys. Res. Lett., *27*, 705–707.

Gill, A. E. 1982. Atmosphere -Ocean Dynamics, Academic Press, 662 pp.

Hollowed, A. B. and W. S. Wooster. 1992. Variability of winter ocean conditions and strong year classes of northeast Pacific groundfish. ICES Marine Science Symposium, *195*, 433–444.

Jacobs, G. A., H. E. Hulburt, J. C. Kindle, E. J. Metzger, J. L. Mitchell, W. J. Teague and A. J. Wallcraft. 1994. Decade-scale trans-Pacific propagation and warming effect of an El Niño anomaly. Nature, *370*, 360–363.

Jiménez-Pérez, L. C. and J. R. Lara-Lara. 1988. Zooplankton biomass and copepod community structure in the Gulf of California during the 1982–1983 El Niño event. CalCOFI Report, *12*, 122–128.

Kahru, M., S. G. Marinone, S. E. Lluch-Cota, A. Parés-Sierra and B. G. Mitchell. 2004. Ocean-color variability in the Gulf of California: Scales from days to ENSO. Deep-Sea Res. II, *51*, 139–146.

Latif, M. and T. P. Barnett. 1994. Causes of decadal climate variability over the North Pacific and North America. Science, *266*, 634–637.

Lavaniegos-Espejo, B. and J. R. Lara-Lara. 1990. Zooplankton of the Gulf of California after the 1982–1983 El Niño event: Biomass distribution and abundance. Pacific Science, *44*, 297–310.

Lavín, M. F., E. Palacios-Hernandez and C. Cabrera. 2003. Sea surface temperature anomalies and trend in the Gulf of California, *in* Effects of El Niño in México. Geofísica Internacional-Special volume, *42*, 363–375.

Lluch-Cota, D. B., W. S. Wooster and S. R. Hare. 2001. Sea surface temperature variability in coastal areas of the northeastern Pacific related to the El Niño-Southern Oscillation and Pacific Decadal Oscillation. Geophys. Res. Lett., *28*, 2029–2032.

Lluch-Cota, D. B., W. S. Wooster, S. R. Hare, D. Lluch-Belda and A. Parés-Sierra. 2003. Principal modes and related frequencies of sea surface temperatures variability in the Pacific Coast of North America. J. Oceanogr., *59*, 477–488.

Lluch-Cota, S. E. 2000. Coastal upwelling in the eastern Gulf of California. Oceanologica Acta, *23*, 731–740.

Lluch-Cota, S. E., E. A. Aragón-Noriega, F. Arreguin-Sánchez, D. Aurioles-Gamboa, J. Bautista-Romero, R. C. Brusca, R. Cervantes-Duarte, R. Cortéz-Altamirano, P. Del-Monte-Luna, A. Esquivel-Herrera, G. Fernández, M. E. Hendrickx, S. Hernandez-Vázquez, H. Herrera-Cervantes, M. Kahru, M. Lavin, D. Lluch-Belda, D. Lluch-Cota, J. Lopez-Martínez, S. G. Marinone, M. O. Nevárez-Martínez, S. Ortega-García, E. Palacios-Castro, A. Parés-Sierra, G. Ponce-Díaz, M. Ramírez-Rodríguez, C. A. Salinas-Zavala, R. A. Schwartzlose and A. P. Sierra-Beltrán. 2007. The Gulf of California: Review of ecosystem status and sustainability challenges. Prog. Oceanogr., doi: 10.1016/j. pocean. 2007.01.013.

Mantua, N. J. 2001. The Pacific decadal oscillation, *in* The Encyclopedia of Global Environmental Change, Vol. 1: The Earth System: Physical and Chemical Dimension of Global Environmental Change, M. C. McCracken and J. S. Perry, eds., 592–594.

Marinone. S. G. 1988. A note on non-seasonal variability in the central Gulf of California. Ciencias Marinas, *115*, 887–913.

North, G. R., T. L. Bell, R. F. Calahan and F. J. Moeng. 1982. Sampling errors in the estimation of empirical orthogonal functions. Mon. Weath. Rev., *110*, 699–706.

Paden, C. A., C. D. Winant and M. Abbott. 1991. Tidal and atmospheric forcing of the upper ocean in the Gulf of California 1. Sea surface temperatures variability. J. Geophys. Res., *96*, 18337–18359.

Parés-Sierra, A., A. Mascarenhas, S. G. Marinone and R. Castro. 2003. Temporal and spatial variation of the surface winds in the Gulf of California. Geophys. Res. Lett., *30*, 451–454.

Parés-Sierra, A. and J. J. O'Brien. 1989. The seasonal and interannual variability of the California Current System: A numerical model. J. Geophys. Res., *93*, 3159–3180.

Peixoto, J. P. and A. H. Oort. 1992. Physics of Climate, American Institute of Physics, 520 pp.

Ripa, P. 1997. Toward a physical explanation of the seasonal dynamics and thermodynamics of the Gulf of California. J. Phys. Oceanogr., *27*, 597–614.

Ripa, P. and S. G. Marinone. 1989. Seasonal variability of temperature, salinity, velocity, vorticity and sea level in the central Gulf of California, as inferred from historical data. Q. J. Roy. Meteor. Soc., *115*, 887–913.

Robles J. M. and S. G. Marinone. 1987. Seasonal and interannual thermohaline variability in the Guaymas Basin of the Gulf of California. Cont. Res. Sci., *7*, 715–733.

Ryan, H. F. and M. Noble. 2002. Sea level response to ENSO along the central California coast: how the 1997–1998 event compares with the historic record. Prog. Oceanogr., *54,* 149–169.

Santamaria-del-Angel, E. and S. Alvarez-Borrego. 1994. Gulf of California biogeographic regions based on coastal zone color scanner imagery. J. Geophys. Res., *99*, 7411–7421.

Soto-Mardones, L., S. G. Marinote and A. Parés-Sierra. 1999. Time and spatial variability of sea surface temperature in the Gulf of California. Ciencias Marinas, *25,* 1–30.

Strub, P. T. and C. James. 2002. Altimeter-derived surface circulation in the large-scale Pacific gyres. Part 2: 1997–1998 El Niño anomalies. Prog. Oceanogr., *53*, 185–214.

Subbotina, M. M., R. E. Thomson and A. B. Rabinovich. 2001. Spectral characteristics of sea level variability along the coast of North America during the 1982–83 and 1997–98 El Niño events. Prog. Oceanogr., *49*, 353–372.

Thunell, R. 1998. Seasonal and annual variability in particle fluxes in the Gulf of California: A response to climate forcing. Deep-Sea Res. I, *45*, 2059–2083.

Tribbia J. J. 1991. The rudimentary theory of atmospheric teleconnections associated with ENSO, *in* Teleconnections linking worldwide climate anomalies. Scientific basis and societal impacts, M. H. Glantz, R. K. Waltz and N. Nicholls, eds., Cambridge University Press, NY, 285–307.

Valdez-Holguín, J. E. 1986. Distribución de la biomasa y productividad del fitoplancton en el Golfo de California durante el evento de El Niño 1982–1983, M.S. Thesis Cent. de Invest. Cient. y Educ. Super. de Ensenada, Ensenada, Baja California, Mexico, 90 pp.

Wilks, D. S. 1995. Statistical methods in the atmospheric sciences: An introduction. International Geophysics Series, *59*, Academic Press, 464 pp.

Wolter, K. and M. S. Timlin. 1993. Monitoring ENSO in COADS with a seasonally adjusted principal component index. Proc. 17th Climate Dynamics Workshop; Norman, OK, NOAA/NMC/CAC, NSSL, Oklahoma Clim. Survey, CIMMS and School of Meteorology. Univ. Oklahoma, 52–57.

Wooster, W. S. and A. B. Hollowed. 1995. Decadal scale variations in the eastern subarctic Pacific. I. Winter ocean conditions. Climate change and northern fish populations, R. J. Beamish, ed., Canadian Special Publication of Fisheries Aquatic Sciences, *121*, 81–85.

Received: *16 February, 2007*; revised: *9 August, 2007*.